Revisiting Multimode Coupled Bridge Flutter: Some New Insights

Xinzhong Chen[1] and Ahsan Kareem[2]

Abstract: Better understanding of the bimodal coupled bridge flutter involving fundamental vertical bending and torsional modes offers valuable insight into multimode coupled flutter, which has primarily been the major concern in the design of long span bridges. This paper presents a new framework that provides closed-form expressions for estimating modal characteristics of bimodal coupled bridge systems and for estimating the onset of flutter. Though not intended as a replacement for complex eigenvalue analysis, it provides important physical insight into the role of self-excited forces in modifying bridge dynamics and the evolution of intermodal coupling with increasing wind velocity. The accuracy and effectiveness of this framework are demonstrated through flutter analysis of a cable-stayed bridge. Based on this analysis scheme, the role of bridge structural and aerodynamic characteristics on flutter, which helps to better tailor the structural systems and deck sections for superior flutter performance, is emphasized. Accordingly, guidance on the selection of critical structural modes and the role of different force components in multimode coupled flutter are delineated. The potential significance of the consideration of intermodal coupling in predicting torsional flutter is highlighted. Finally, clear insight concerning the role of drag force to bridge flutter is presented.

DOI: 10.1061/(ASCE)0733-9399(2006)132:10(1115)

CE Database subject headings: Flutter; Wind loads; Aerodynamics; Aeroelasticity; Dynamics; Bridges.

Introduction

Flutter instability is primarily one of the major concerns in the design of long span bridges. The flutter analysis that combines a finite-element model of the bridge and its aerodynamic characteristics derived from section model wind tunnel tests has played an important role in seeking design solutions for innovative aerodynamically tailored bridge decks and effective structural systems. The mode-by-mode approach that neglects intermodal aerodynamic coupling has proven its utility in predicting bridge flutter dominated by the action of a single mode (Scanlan 1978). However, experience shows that bridges with longer spans generally require a multimode coupled analysis framework (e.g., Jones et al. 1998; Chen et al. 2000a). In this context, time domain analysis schemes facilitate consideration of nonlinearities in both structural and aerodynamic characteristics and the influence of turbulence on flutter (Diana et al. 1999; Chen et al. 2000b; Chen and Kareem 2003a,b).

The multimode coupled bridge flutter is often dominated by the aerodynamic coupling of fundamental vertical bending and torsional modes with secondary contributions from other modes (Chen et al. 2000a). Therefore, better understanding of the bimodal flutter involving the fundamental vertical bending and torsional modes promises to provide valuable insight into multimode coupled flutter. The bimodal coupled flutter has laid a firm foundation for developing spring-supported bridge section model tests in wind tunnels as a valuable tool for flutter prediction. The bimodal flutter analysis is also often performed at preliminary design stages to seek the best solution for superior flutter performance. A step-by-step iterative analysis framework for the bimodal coupled flutter was introduced by Matsumoto et al. (1997) and Matsumoto (1999), which attempted to capture the mechanism surrounding the evolution of bridge flutter.

The self-excited lift and pitching moment on a bridge deck caused by vertical and torsional motions have been considered as the most important force components in the prediction of bridge flutter, whereas the lift force and pitching moment on a bridge deck induced by the lateral motion and drag force have been generally regarded as less important. However, recent experience involving the Akashi Kaikyo Bridge has revealed that the drag force induced by the torsional displacement resulted in a considerable level of negative damping at higher wind velocities, which is responsible for the coupled flutter (Miyata et al. 1994). Since then, the need for modeling and measurements of drag force and its potential importance to bridge flutter analysis have received some attention in the literature (e.g., Jones et al. 1998, 2002). However, a fundamental understanding of this behavior has remained unclear in the bridge aerodynamics community.

In this paper, a new analysis framework that offers closed-form expressions for estimating bimodal coupled flutter is presented. Its accuracy and effectiveness are demonstrated through the flutter analysis of a cable-stayed bridge. Subsequently, this framework is utilized to emphasize the significance of bridge structural and aerodynamic characteristics on flutter. Based on

[1]Assistant Professor, Wind Science and Engineering Research Center, Dept. of Civil Engineering, Texas Tech Univ., Lubbock, TX 79409. E-mail: xinzhong.chen@ttu.edu

[2]Professor, Dept. of Civil and Environmental Engineering and Geological Sciences, Univ. of Notre Dame, Notre Dame, IN 46556. E-mail: kareem@nd.edu

Note. Associate Editor: Nicos Makris. Discussion open until March 1, 2007. Separate discussions must be submitted for individual papers. To extend the closing date by one month, a written request must be filed with the ASCE Managing Editor. The manuscript for this paper was submitted for review and possible publication on September 7, 2004; approved on February 22, 2006. This paper is part of the ***Journal of Engineering Mechanics***, Vol. 132, No. 10, October 1, 2006. ©ASCE, ISSN 0733-9399/2006/10-1115–1123/$25.00.

this framework, guidance on the selection of critical structural modes and the role of different force components in multimode coupled flutter are delineated. The potential importance of the consideration of intermodal coupling in predicting torsional flutter is highlighted. Finally, a clear insight concerning the role of drag force in bridge flutter is presented.

New Analysis Framework

The bridge deck dynamic displacements in the vertical, lateral, and torsional directions, i.e., $h(x,t)$, $p(x,t)$, and $\alpha(x,t)$, respectively, about its statically displaced position, are expressed as

$$h(x,t)=\sum_j h_j(x)q_j(t);\quad p(x,t)=\sum_j p_j(x)q_j(t);$$
$$\alpha(x,t)=\sum_j \alpha_j(x)q_j(t) \tag{1}$$

where $h_j(x)$, $p_j(x)$ and $\alpha_j(x)=j$th mode shapes in each respective direction; $q_j(t)=j$th modal coordinate; and $x=$spanwise position.

The self-excited (se) forces per unit length linearized around the statically displaced position, i.e., lift (downward), drag (downwind), and pitching moment (nose up), are given as (e.g., Scanlan 1978, 1993; Chen and Kareem 2002)

$$L_{se}(t)=\frac{1}{2}\rho U^2(2b)\times\left(kH_1^*\frac{\dot{h}}{U}+kH_2^*\frac{b\dot{\alpha}}{U}+k^2H_3^*\alpha+k^2H_4^*\frac{h}{b}+kH_5^*\frac{\dot{p}}{U}+k^2H_6^*\frac{p}{b}\right) \tag{2}$$

$$D_{se}(t)=\frac{1}{2}\rho U^2(2b)\times\left(kP_1^*\frac{\dot{p}}{U}+kP_2^*\frac{b\dot{\alpha}}{U}+k^2P_3^*\alpha+k^2P_4^*\frac{p}{b}+kP_5^*\frac{\dot{h}}{U}+k^2P_6^*\frac{h}{b}\right) \tag{3}$$

$$M_{se}(t)=\frac{1}{2}\rho U^2(2b^2)\times\left(kA_1^*\frac{\dot{h}}{U}+kA_2^*\frac{b\dot{\alpha}}{U}+k^2A_3^*\alpha+k^2A_4^*\frac{h}{b}+kA_5^*\frac{\dot{p}}{U}+k^2A_6^*\frac{p}{b}\right) \tag{4}$$

where $\rho=$air density; $U=$mean wind velocity; $B=2b=$bridge deck width; $k=\omega b/U=$reduced frequency; $\omega=$frequency of motion; and H_j^*, P_j^*, and A_j^* $(j=1,2,\ldots,6)=$flutter derivatives that are functions of reduced frequency.

The governing matrix equation of bridge motions in terms of modal coordinates is given by

$$\mathbf{M}\ddot{\mathbf{q}}+\mathbf{C}\dot{\mathbf{q}}+\mathbf{K}\mathbf{q}=\frac{1}{2}\rho U^2\left(\mathbf{A}_s\mathbf{q}+\frac{b}{U}\mathbf{A}_d\dot{\mathbf{q}}\right) \tag{5}$$

where $\mathbf{M}=\text{diag}[m_j]$, $\mathbf{C}=\text{diag}[2m_j\xi_{sj}\omega_{sj}]$ and $\mathbf{K}=\text{diag}[m_j\omega_{sj}^2]$ $=$generalized mass, damping, and stiffness matrices, respectively; m_j, ξ_{sj}, and $\omega_{sj}=j$th modal mass, damping ratio, and frequency; $\mathbf{A}_s$ and $\mathbf{A}_d=$aerodynamic stiffness and damping matrices, respectively, and their elements pertaining to the i and jth modes are given by

$$A_{sij}=(2k^2)(H_4^*G_{h_ih_j}+H_6^*G_{h_ip_j}+bH_3^*G_{h_i\alpha_j}+P_6^*G_{p_ih_j}+P_4^*G_{p_ip_j}+bP_3^*G_{p_i\alpha_j}+bA_4^*G_{\alpha_ih_j}+bA_6^*G_{\alpha_ip_j}+b^2A_3^*G_{\alpha_i\alpha_j}) \tag{6}$$

$$A_{dij}=(2k)(H_1^*G_{h_ih_j}+H_5^*G_{h_ip_j}+bH_2^*G_{h_i\alpha_j}+P_5^*G_{p_ih_j}+P_1^*G_{p_ip_j}+bP_2^*G_{p_i\alpha_j}+bA_1^*G_{\alpha_ih_j}+bA_5^*G_{\alpha_ip_j}+b^2A_2^*G_{\alpha_i\alpha_j}) \tag{7}$$

and $G_{r_is_j}=\int_{\text{span}}r_i(x)s_j(x)dx$ (where $r,s=h,p,\alpha$)$=$modal integrals.

The modal frequencies and damping ratios as well as intermodal coupling of the bridge at a given wind velocity, with the contributions of aerodynamic stiffness and damping terms, can be analyzed through the solution of the following complex eigenvalue problem by putting $\mathbf{q}(t)=\mathbf{q}_0e^{\lambda t}$:

$$(\lambda^2\mathbf{M}+\lambda\mathbf{C}+\mathbf{K})\mathbf{q}_0e^{\lambda t}=\frac{1}{2}\rho U^2(\mathbf{A}_s+\bar{\lambda}\mathbf{A}_d)\mathbf{q}_0e^{\lambda t} \tag{8}$$

where $\lambda=-\xi\omega+i\omega\sqrt{1-\xi^2}$; ξ and $\omega=$damping ratio and frequency of the complex modal branch of interest; $\bar{\lambda}=\lambda b/U=(-\xi+i\sqrt{1-\xi^2})k$; and $i=\sqrt{-1}$. The flutter condition is determined by seeking the flutter onset velocity that corresponds to zero damping.

Now, consider the bimodal coupled case where the bridge is modeled by its fundamental vertical bending and torsional modes, i.e., $h_1(x)\neq 0$, $p_1(x)=0$, $\alpha_1(x)=0$; $h_2(x)=0$, $p_2(x)\neq 0$, $\alpha_2(x)\neq 0$; and $\mathbf{q}_0=\{q_{10}q_{20}\}^T$ (where $T=$matrix transpose operator). In this context where the fundamental torsional mode is antisymmetric, the corresponding fundamental bending mode is referred to as the fundamental antisymmetric mode. Otherwise, both are referred to as fundamental symmetric modes. In the ensuing analysis, only the lift and pitching moment caused by the vertical and torsional motions are considered. Accordingly, the aerodynamic matrices are described by

$$\mathbf{A}_s=(2k^2)\begin{bmatrix}H_4^*G_{h_1h_1} & bH_3^*G_{h_1\alpha_2}\\ bA_4^*G_{h_1\alpha_2} & b^2A_3^*G_{\alpha_2\alpha_2}\end{bmatrix} \tag{9}$$

$$\mathbf{A}_d=(2k)\begin{bmatrix}H_1^*G_{h_1h_1} & bH_2^*G_{h_1\alpha_2}\\ bA_1^*G_{h_1\alpha_2} & b^2A_2^*G_{\alpha_2\alpha_2}\end{bmatrix} \tag{10}$$

The aeroelastic bridge system with low level of damping is considered. Because of low level of damping, the decay or growth of motion has little influence on the generation of the self-excited forces, i.e., $\mathbf{A}_s+\bar{\lambda}\mathbf{A}_d\approx\mathbf{A}_s+(ik)\mathbf{A}_d$. By eliminating the terms involving higher order of damping ratio, i.e., $\lambda^2\approx-\omega^2-2\xi\omega i$, $2\xi_{s1}\omega_{s1}\lambda\approx 2\xi_{s1}\omega_{s1}\omega i$ and $2\xi_{s2}\omega_{s2}\lambda\approx 2\xi_{s2}\omega_{s2}\omega i$, Eq. (8) can be rewritten as

$$[-\omega^2+i2\bar{\xi}_1\bar{\omega}_1\omega+\bar{\omega}_1^2]q_{10}e^{\lambda t}=\mu D\omega^2(H_3^*+iH_2^*)(G_{\alpha_2\alpha_2}/G_{h_1h_1})^{1/2}(bq_{20})e^{\lambda t} \tag{11}$$

$$[-\omega^2+i2\bar{\xi}_2\bar{\omega}_2\omega+\bar{\omega}_2^2](bq_{20})e^{\lambda t}=\upsilon D\omega^2(A_4^*+iA_1^*)(G_{h_1h_1}/G_{\alpha_2\alpha_2})^{1/2}bq_{10}e^{\lambda t} \tag{12}$$

where $\bar{\omega}_j$ and $\bar{\xi}_j$ $(j=1,2)=$frequencies and damping ratios that are influenced only by the uncoupled self-excited forces, i.e., the lift caused by vertical motion and the pitching moment caused by torsion, associated with H_1^*, H_4^*, A_2^*, and A_3^*

$$\bar{\omega}_1 = \omega_{s1}[1 - \mu(\omega/\omega_{s1})^2 H_4^*]^{1/2} \tag{13}$$

$$\bar{\xi}_1 = \xi_{s1}(\omega_{s1}/\bar{\omega}_1) - 0.5\mu(\omega/\bar{\omega}_1)H_1^* - \xi(\omega/\bar{\omega}_1) \tag{14}$$

$$\bar{\omega}_2 = \omega_{s2}[1 - \upsilon(\omega/\omega_{s2})^2 A_3^*]^{1/2} \tag{15}$$

$$\bar{\xi}_2 = \xi_{s2}(\omega_{s2}/\bar{\omega}_2) - 0.5\upsilon(\omega/\bar{\omega}_2)A_2^* - \xi(\omega/\bar{\omega}_2) \tag{16}$$

and $\mu=\rho b^2/m$; $\upsilon=\rho b^4/I$; $m=m_1/G_{h_1h_1}$; and $I=m_2/G_{\alpha_2\alpha_2}=mr^2$ =effective mass and polar moment of inertia per unit span, respectively; r=radius of gyration of the cross section; $D=G_{h_1\alpha_2}/(G_{h_1h_1}G_{\alpha_2\alpha_2})^{1/2}$=the similarity factor between the vertical and torsional mode shapes.

When the coupled self-excited forces, i.e., the lift caused by torsion and the pitching moment caused by vertical motion, associated with H_2^*, H_3^*, A_1^*, and A_4^*, are negligibly small, the equations of motion become uncoupled. For this uncoupled system, the modal frequencies and damping ratios are given by (Scanlan 1978)

$$\omega_{10} = \omega_{s1}(1 + \mu H_4^*)^{-1/2} \tag{17}$$

$$\xi_{10} = \xi_{s1}(\omega_{s1}/\omega_{10}) - 0.5\mu H_1^* \tag{18}$$

$$\omega_{20} = \omega_{s2}(1 + \upsilon A_3^*)^{-1/2} \tag{19}$$

$$\xi_{20} = \xi_{s2}(\omega_{s2}/\omega_{20}) - 0.5\upsilon A_2^* \tag{20}$$

It is noted that in the case of the uncoupled system, $\omega_{10}=\bar{\omega}_1$, $\bar{\xi}_1=0$, $\omega_{20}=\bar{\omega}_2$, and $\bar{\xi}_2=0$. As the flutter derivatives are functions of reduced frequency, for the bimodal coupled system, $\bar{\omega}_1 \neq \omega_{10}$ and $\bar{\omega}_2 \neq \omega_{20}$. However, the modal frequencies of the coupled system are generally very close to those of the corresponding uncoupled system at the same wind velocity. In addition, the influence of the uncoupled self-excited forces on modal frequencies is not sensitive to the change in reduced frequency. Therefore, $\bar{\omega}_1 \approx \omega_{s1}[1-\mu(\bar{\omega}_1/\omega_{s1})^2 H_4^*]^{1/2}=\omega_{10}$ and $\bar{\omega}_2 \approx \omega_{s2}[1-\upsilon(\bar{\omega}_2/\omega_{s2})^2 A_3^*]^{1/2}=\omega_{20}$.

The solutions of Eqs. (11) and (12) lead to the modal frequencies, damping ratios, and complex mode shapes for both modal branches. Consider the solution of the vertical mode branch with a frequency $\omega=\omega_1$ that is closer to $\bar{\omega}_1$ than $\bar{\omega}_2$, and damping ratio $\xi=\xi_1$. The amplitude ratio, Φ, and phase difference between vertical and torsional motions, ϕ, as defined by $bq_{20}/q_{10}=\Phi e^{i\phi}$, can be determined from Eq. (12) as

$$\Phi = \upsilon D R_{d1}\{[(A_4^*)^2 + (A_1^*)^2][G_{h_1h_1}/G_{\alpha_2\alpha_2}]\}^{1/2} \tag{21}$$

$$\phi = \tan^{-1}(A_1^*/A_4^*) - \tan^{-1}\{[2\bar{\xi}_2(\omega_1/\bar{\omega}_2)]/[1 - (\omega_1/\bar{\omega}_2)^2]\} \tag{22}$$

where

$$R_{d1} = (\omega_1/\bar{\omega}_2)^2\{[1 - (\omega_1/\bar{\omega}_2)^2]^2 + [2\bar{\xi}_2(\omega_1/\bar{\omega}_2)]^2\}^{-1/2} \tag{23}$$

By replacing (bq_{20}) with $q_{10}\Phi e^{i\phi}$, Eq. (11) becomes

$$[-\omega_1^2 + i2\bar{\xi}_1\bar{\omega}_1\omega_1 + \bar{\omega}_1^2 - \mu\upsilon D^2\omega_1^2\Phi' e^{i\phi'}]q_{10}e^{\lambda t} = 0 \tag{24}$$

where

$$\Phi' = R_{d1}\{[(H_3^*)^2 + (H_2^*)^2][(A_4^*)^2 + (A_4^*)^2]\}^{1/2} \tag{25}$$

$$\phi' = \tan^{-1}(H_2^*/H_3^*) + \phi \tag{26}$$

Eq. (24) can only be satisfied when the term in the brackets becomes zero, which leads to the closed-form solutions for the frequency and damping ratio of the modal branch as

$$\omega_1 = \omega_{s1}(1 + \mu H_4^* + \mu\upsilon D^2\Phi' \cos\phi')^{-1/2} \tag{27}$$

$$\xi_1 = \xi_{s1}(\omega_{s1}/\omega_1) - 0.5\mu H_1^* - 0.5\mu\upsilon D^2\Phi' \sin\phi' \tag{28}$$

Similar expressions can be derived for the torsional modal branch with a frequency $\omega=\omega_2$ that is closer to $\bar{\omega}_2$ than $\bar{\omega}_1$, and damping ratio $\xi=\xi_2$. The amplitude ratio, Ψ, and phase difference between vertical and torsional motions, ψ, as defined by $q_{10}/(bq_{20})=\Psi e^{i\psi}$, can be determined from Eq. (11) as

$$\Psi = \mu D R_{d2}\{[(H_3^*)^2 + (H_2^*)^2][G_{\alpha_2\alpha_2}/G_{h_1h_1}]\}^{1/2} \tag{29}$$

$$\psi = \tan^{-1}(H_2^*/H_3^*) - \tan^{-1}\{[2\bar{\xi}_1(\omega_2/\bar{\omega}_1)]/[1 - (\omega_2/\bar{\omega}_1)^2]\} \tag{30}$$

where

$$R_{d2} = (\omega_2/\bar{\omega}_1)^2\{[1 - (\omega_2/\bar{\omega}_1)^2]^2 + [2\bar{\xi}_1(\omega_2/\bar{\omega}_1)]^2\}^{-1/2} \tag{31}$$

The frequency and damping ratio of this modal branch are given by

$$\omega_2 = \omega_{s2}(1 + \upsilon A_3^* + \mu\upsilon D^2\Psi' \cos\psi')^{-1/2} \tag{32}$$

$$\xi_2 = \xi_{s2}(\omega_{s2}/\omega_2) - 0.5\upsilon A_2^* - 0.5\mu\upsilon D^2\Psi' \sin\psi' \tag{33}$$

where

$$\Psi' = R_{d2}\{[(H_3^*)^2 + (H_2^*)^2][(A_4^*)^2 + (A_1^*)^2]\}^{1/2} \tag{34}$$

$$\psi' = \tan^{-1}(A_1^*/A_4^*) + \psi \tag{35}$$

It is noted that the derivation of the preceding closed-form expressions was based only on the assumption of low level of damping. In fact, such an approximation has also been implicitly invoked in the modeling of the self-excited forces and analysis of bridge flutter. Because of the low level of damping, the decay or growth of the deck motion does not influence the self-excited forces, which permits characterization of flutter derivatives only in terms of the reduced frequency rather than both the reduced frequency and damping. This assumption has also been routinely made in flutter analysis schemes such as so-called $p-k$ and p methods and conventional complex eigenvalue analysis (e.g., Chen and Kareem 2003b). Therefore, this approximation is by no means restrictive, thus the proposed framework with closed-form expressions is expected to be generally applicable to a variety of bimodal coupled systems. It is also emphasized that at the flutter onset velocity with zero damping, the proposed framework for the flutter modal branch results in the exact solution as the conventional eigenvalue analysis because the invoked approximation vanishes.

As the flutter derivatives are functions of reduced frequency, in the preceding expressions for each modal branch, the flutter derivatives are defined at the respective reduced frequency. The influence of the coupled self-excited forces on the modal frequencies is often negligible, while it tends to separate closely spaced frequencies. The influence of damping ratio ξ on the amplitude ratio and phase difference is often small and even can be neglected by simply setting $\xi=0$, particularly, in cases where modal frequencies are well separated and the damping ratio is small. Although iterative calculations for both frequencies and damping ratios are required, they converge very fast. The iterative calculations may even be eliminated by inserting respective values

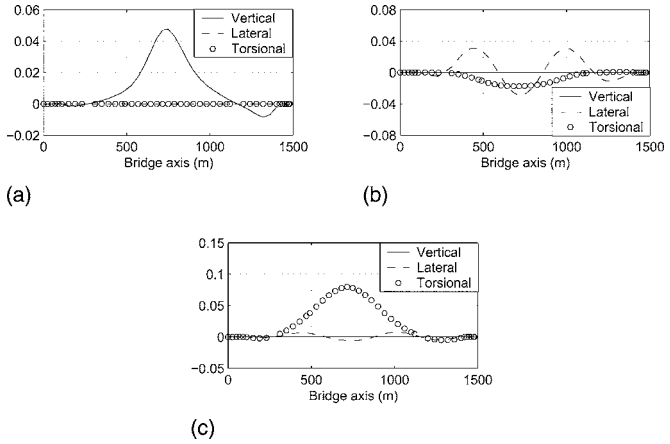

Fig. 1. Bridge mode shapes: (a) Mode 3; (b) Mode 10; and (c) Mode 13

of frequencies and damping ratios obtained at the immediate previous wind velocity for evaluating parameters, like the flutter derivatives, on the right-hand side of the formulations. It is emphasized that the proposed framework is not intended to replace the conventional complex eigenvalue analysis framework for the purpose of flutter analysis. Instead, it offers closed-form analytical solutions that provide clear physical insight as to how self-excited forces change bridge dynamics and to how the intermodal coupling evolves with increasing wind velocity.

Illustration and Discussion

In the following, the accuracy and effectiveness of the proposed framework is demonstrated utilizing a long span cable-stayed

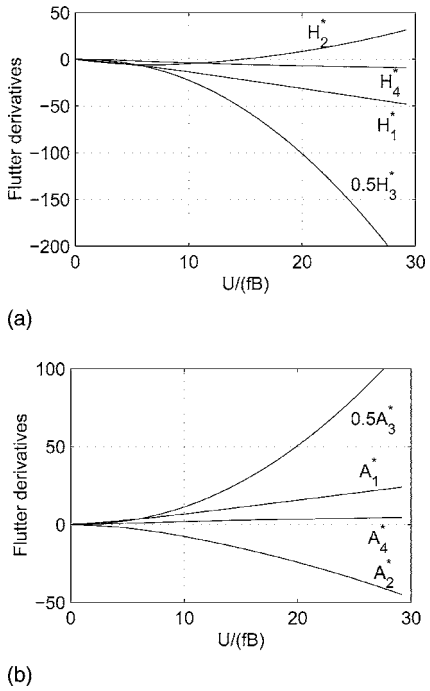

Fig. 2. Flutter derivatives for the slender bridge deck section: (a) flutter derivatives H_i^* $(i=1,2,3,4)$; (b) flutter derivatives A_i^* $(i=1,2,3,4)$

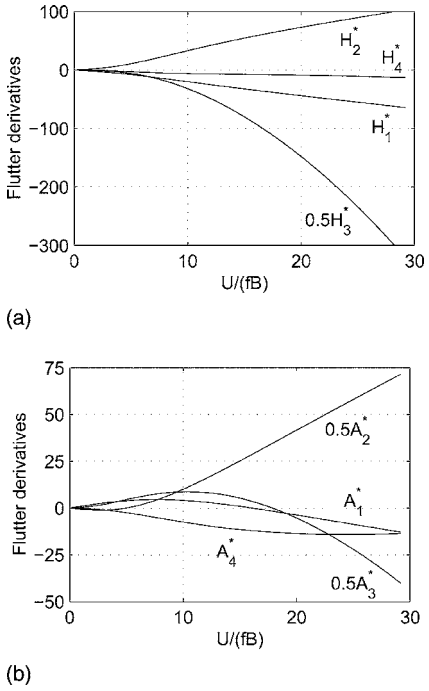

Fig. 3. Flutter derivatives for the relatively bluff bridge deck section: (a) flutter derivatives H_i^* $(i=1,2,3,4)$; (b) flutter derivatives A_i^* $(i=1,2,3,4)$

bridge with a center span of about 1000 m. The bridge deck width is $B=30$ m. The nondimensional mass and polar moment of inertia parameters are $\mu=0.0139$ and $\upsilon=0.0579$. The frequencies of the fundamental vertical bending and torsional modes, i.e., Modes 3 and 13, are 0.2144 and 0.5708 Hz, respectively. The corresponding mode shapes in terms of the bridge deck displacements in three directions are shown in Fig. 1. It can be seen that Mode 3 is a pure vertical bending mode, and Mode 13 is a torsional mode with secondary coupled lateral motion. For these two modes, the modal integrals are $G_{h_1h_1}=0.4951$, $bG_{h_1p_2}=-0.0224$, $bG_{h_1\alpha_2}=0.9767$, $G_{p_2p_2}=0.0213$, and $b^2G_{\alpha_2\alpha_2}=2.0573$. The similarity factor of these two modes is $D=0.9678$, very close to unity, which indicates a high modal similarity in shapes between these two modes. The modal damping ratio for these two modes is assumed to be 0.0032. Only the lift and pitching moment acting on the bridge deck related to flutter derivatives H_i^*, A_i^* $(i=1, 2, 3, 4)$ are considered. For comparison, two typical cases, referred to as Cases A and B, corresponding to a slender and a relatively bluff bridge deck section, respectively, are considered. In Case A, the flutter derivatives are calculated from Theoderson function. As shown in Fig. 2, H_1^*, H_3^*, H_4^*, $A_2^*<0$, and H_2^*, A_1^*, A_3^*, $A_4^*>0$; in Case B, the flutter derivatives are measured using a rectangular section with width to height ratio of 5 (Matsumoto et al. 1997). As shown in Fig. 3, H_1^*, H_3^*, H_4^*, $A_4^*<0$, $H_2^*>0$, $A_1^*>0$, and changes to <0 for higher reduced wind velocities and $A_2^*<0$ at lower reduced wind velocities, but >0 at higher reduced wind velocities, and A_3^* is originally >0, but changes to <0 as the reduced wind velocity increases. Obviously, Cases A and B, respectively, correspond to the cases of coupled flutter and torsional flutter.

Fig. 4 shows the predicted frequencies and damping ratios as well as mode shapes in terms of amplitude ratios and phase differences for both modal branches in Case A. For the vertical modal branch, the complex mode is defined as the ratio of tor-

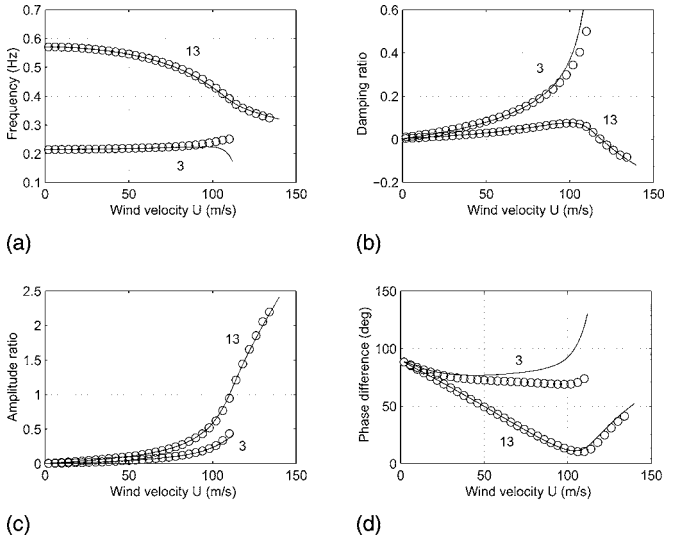

Fig. 4. Comparison of flutter analysis for the cable-stayed bridge (Case A): (a) frequency; (b) damping ratio; (c) amplitude ratio; and (d) phase difference

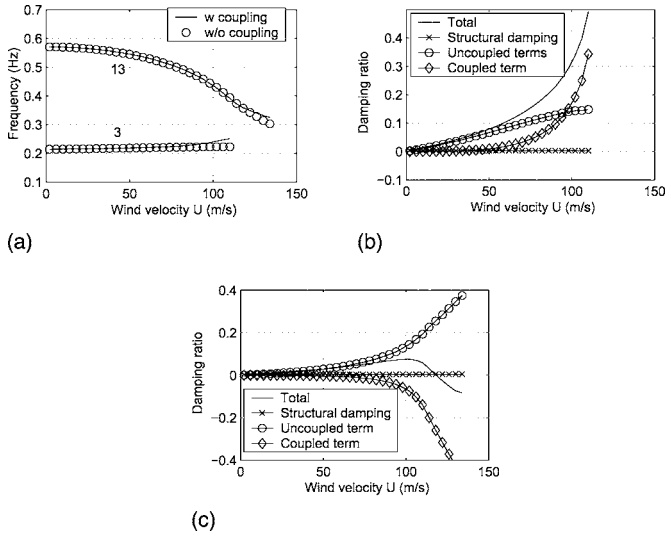

Fig. 6. Contributions of different force components to frequencies and damping ratios (Case A): (a) frequency; (b) damping ratio (Mode Branch 3); and (c) damping ratio (Mode Branch 13)

sional motion to vertical motion, thus a positive value of phase difference suggests that the vertical motion lags the torsional motion. For the torsional mode branch, the complex mode is defined as the ratio of vertical motion to torsional motion, thus a positive value of phase difference suggests that the torsional motion lags the vertical motion. The amplitude ratio is given in terms of the ratio between the vertical and torsional displacements of the bridge deck at the center of the main span so that these are independent of the mode shape normalization scheme. The solid lines and circles, respectively, show the results of the conventional complex eigenvalue analysis and the proposed framework. Fig. 5 shows the results for Case B. It can be seen that the proposed framework provides predictions for both branches that show a good agreement with the conventional complex eigenvalue analysis. The predicted critical flutter velocities by both approaches are identical, i.e., 119 m/s for Case A and 69.6 m/s for Case B.

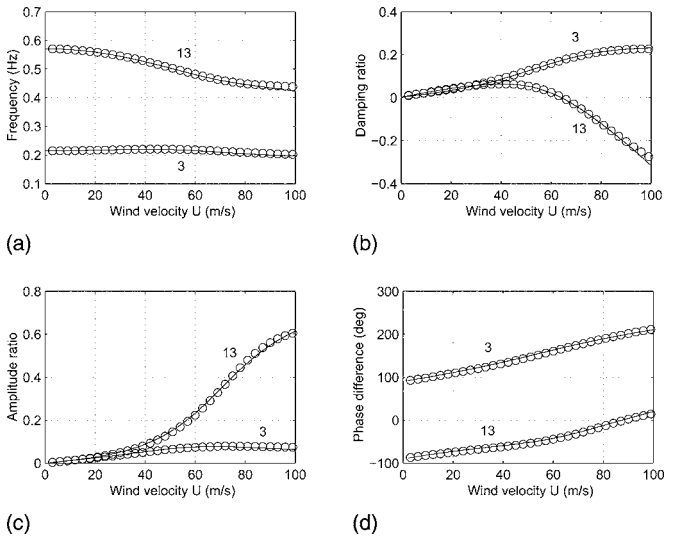

Fig. 5. Comparison of flutter analysis for the cable-stayed bridge (Case B): (a) frequency; (b) damping ratio; (c) amplitude ratio; and (d) phase difference

There are some minor differences between the two approaches in Case A, which only surface at the high wind velocities for the vertical modal branch with high levels of damping where the invoked assumption breaks down. It should be mentioned that the flutter derivatives are generally experimentally identified for motions with low level of damping (free vibration method) or zero damping (forced vibration method). Therefore, the predicted high level of damping even by the conventional eigenvalue analysis is equally questionable.

Significance of Bridge Structural and Aerodynamic Characteristics on Flutter

The proposed framework clearly highlights the contributions of different aerodynamic force components to the modifications in modal frequencies and damping ratios with changing wind velocities. For the example of the torsional modal branch, the terms υA_3^* and $-0.5\upsilon A_2^*$ in Eqs. (32) and (33), respectively, represent the influences of uncoupled aerodynamic stiffness and damping forces on the frequency and damping. The terms involving $\mu\upsilon D^2\Psi' \sin\psi'$ and $-0.5\mu\upsilon D^2\Psi' \cos\psi'$ are the respective contributions from the coupled aerodynamic forces. Fig. 6 shows the contributions of different force components to the modal frequencies and damping ratios in Case A. It is inferred from Fig. 6(a) that the modification in frequencies is a result of the uncoupled aerodynamic stiffness, while the contribution of coupled aerodynamic forces is quite small. As shown in Fig. 6(b), the coupled aerodynamic forces result in an increase in the damping of the vertical modal branch. By contrast, as shown in Fig. 6(c), the coupled forces generate negative damping in the torsional modal branch, which leads to the initiation of coupled flutter at 119 m/s. As $A_2^* < 0$, torsional motion generates positive damping and torsional flutter does not exist at the action of the torsional mode alone. The contrasting contributions of the coupled aerodynamic forces to the damping ratios of both modal branches clearly point at an energy transfer between these two branches.

This contrasting behavior is attributed to the difference in the algebraic signs of $\sin\phi'$ and $\sin\psi'$, respectively, for the ver-

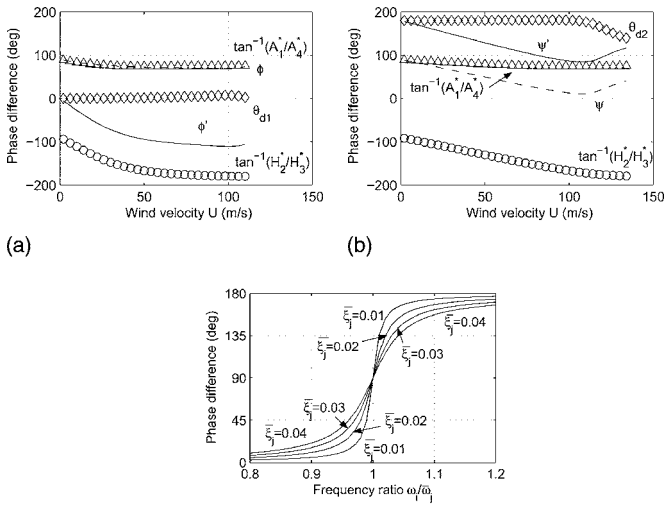

Fig. 7. Phase differences due to structural and aerodynamic characteristics (Case A): (a) vertical modal branch; (b) torsional modal branch; and (c) θ_{d1} and θ_{d2}

tical and torsional modal branches, where $\phi' = \tan^{-1}(H_2^*/H_3^*) + \tan^{-1}(A_1^*/A_4^*) - \theta_{d1}$, $\psi' = \tan^{-1}(H_2^*/H_3^*) + \tan^{-1}(A_1^*/A_4^*) - \theta_{d2}$, $\theta_{d1} = \tan^{-1}\{[2\bar{\xi}_2(\omega_1/\bar{\omega}_2)]/[1-(\omega_1/\bar{\omega}_2)^2]\}$, and

$$\theta_{d2} = \tan^{-1}\{[2\bar{\xi}_1(\omega_2/\bar{\omega}_1)]/[1-(\omega_2/\bar{\omega}_1)^2]\}$$

The angle $\tan^{-1}(H_2^*/H_3^*)$ represents the phase difference between the torsional motion and its resulting lift force. The angle $\tan^{-1}(A_1^*/A_4^*)$ represents the phase difference between the vertical motion and its resulting pitching moment. As shown in Figs. 7(a and b), $\tan^{-1}(H_2^*/H_3^*)$ for both branches at the same wind velocity are very close to each other, although they correspond to different reduced frequencies. Similar observation can also be made for $\tan^{-1}(A_1^*/A_4^*)$. However, the angles θ_{d1} and θ_{d2}, respectively, for the vertical and torsional branches, are considerably different, which are attributed to the distinct values of frequency ratios, i.e., $\omega_1/\bar{\omega}_1$ and $\omega_2/\bar{\omega}_1$. As shown in Fig. 7(c), for the vertical modal branch, as $\omega_1/\bar{\omega}_2 < 1$, θ_{d1} ranges from 0 to $\pi/2$, and approaches zero for a low level of damping $\bar{\xi}_2$ and a small value of frequency ratio $\omega_1/\bar{\omega}_2$. On the other hand, for the torsional modal branch, as $\omega_2/\bar{\omega}_1 > 1$, θ_{d2} ranges from $\pi/2$ to π, and approaches π for a low level of damping $\bar{\xi}_1$ and a large value of frequency ratio $\omega_2/\bar{\omega}_1$. Consequently, the phase differences of coupled motions in both branches, i.e., ϕ and ψ, are between 0 and $\pi/2$. Thus, the vertical modal branch is associated with a coupled motion in which torsional motion lead vertical motion, while the torsional modal branch corresponds to a coupled motion in which torsional motion lags vertical motion. This type of motion allows the coupled self-excited forces to produce a positive damping to the vertical modal branch as $\sin\phi' < 0$, and a negative damping to the torsional modal branch as $\sin\psi' > 0$. The bimodal coupled flutter is likely to be initiated from the branch with higher frequency.

Fig. 8 shows the contributions of different force components to damping ratio of the torsional modal branch in Case B. As A_2^* becomes a positive value from a negative value with increasing wind velocity, a torsional flutter exists beyond 69.6 m/s even with the involvement of only a single torsional mode. While the contribution of the coupled forces is relatively weak, it reduces the damping and leads to a lower flutter onset velocity of

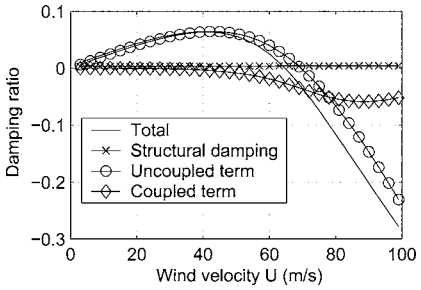

Fig. 8. Contributions of different force components to damping ratio of Modal Branch 13 (Case B)

64.3 m/s. This suggests that the multimode coupled flutter analysis framework is generally required for not only bridges with slender sections but also bridges with relatively bluff sections as has been pointed out in Chen et al. (2000a) and Jones et al. (2002). Consideration of intermodal coupling is potentially more significant in the cases of a soft-type flutter in which negative damping builds up slowly with increasing wind velocity (Chen and Kareem 2003c), and a slight difference in the predicted damping ratio may lead to a notable difference in the predicted critical flutter velocity.

The proposed framework offered intuitive and valuable insight into the significance of structural and aerodynamic characteristics to coupled bridge flutter without performing extensive numerical parametric studies, as is often needed in the traditional framework. These insights could help in developing design solutions to enhance flutter performance. For instance, increases in structural mass and torsional frequency, as well as the frequency ratio between the torsional and vertical modes, help to improve flutter performance. Higher structural damping contributes not only to the increase in the damping of the respective modal branch but also to the reduction of coupled motion and, therefore, is beneficial in delaying flutter. Modification of the structural system can potentially change structural dynamic characteristics including mode shapes, which modify the associated modal integrals and the contributions of aerodynamic forces. The uncoupled self-excited forces due to displacements, i.e., terms related to H_4^* and A_3^*, and in particular A_3^*, reduce the modal frequencies and thus have unfavorable influences on flutter. The uncoupled self-excited forces due to bridge deck velocities, i.e., terms related to H_1^* and A_2^*, and in particular A_2^* increase the modal damping and thus these are beneficial to flutter. The negative damping generated by the coupled forces, i.e., terms related to H_2^*, H_3^*, A_1^*, and A_4^*, and in particular the aerodynamic stiffness terms H_3^* and A_1^*, is the main contributing source that drives the bridge to coupled flutter instability.

In order to improve bridge flutter performance, it is essential to enhance the beneficial features and reduce the unfavorable contributions to system damping. This can be realized through the introduction of aerodynamically tailored bridge decks and effective structural systems. For example, a streamlined multibox section with properly designed large portions of grating/air gap between individual box sections is often characterized by low static drag force and low aerodynamic forces as compared to a single box section without grating/air gap. This kind of section not only offers higher flutter performance but also leads to a relatively soft-type flutter. Additional damping devices can be very effective for further enhancing soft-type flutter behavior (e.g., Chen and Kareem 2003c). In addition, the modification of the bridge cable system of a suspension bridge not only helps in

increasing frequencies, but also has the potential to change mode shapes that could be beneficial to increasing flutter velocity.

The proposed framework also helps to understand the relative participation of structural modes in a multimode coupled flutter, which can guide the selection of modes in a flutter analysis. A mode comprised of large values of coupled aerodynamic stiffness and damping terms with the fundamental torsional mode, which are functions of flutter derivatives and modal integrals, as shown by Eqs. (6) and (7), is more likely to be important for coupled flutter. Furthermore, this coupling will be enhanced when its damping is low and its frequency is close to the torsional modal frequency. For example, the fundamental vertical bending mode often has a higher similarity in shape with the fundamental torsional mode, which leads to larger coupled aerodynamic terms between these two modes. Therefore, the fundamental vertical bending mode is more likely to be coupled with the torsional mode as compared to other higher vertical bending modes whose mode shapes have less similarity with the fundamental torsional mode, although their frequencies may be closer to the torsional modal frequency. Some modes may become locally important at a certain wind velocity range when their frequencies become close to the torsional modal frequency. The modes that are most likely to be excited should be considered in the analysis. The information concerning modes that play a major role in flutter not only helps in better understanding multimode coupled bridge flutter, but it offers equally valuable guidance for design and interpretation of wind tunnel studies using full aeroelastic bridge models, which may only be able to replicate a limited number of selective modes of the prototype bridge due to difficulties in model fabrication.

Influence of Intermodal Coupling on Torsional Flutter

Fig. 9 shows the predicted frequencies and damping ratios of Modal Branches 3, 10, and 13 for the cable-stayed bridge with the bluff deck section (Case B). As shown in Fig. 1(b), Mode 10 is the second symmetric lateral bending mode with coupled motion in torsion. The values of modal integrals of Mode 10 are: $G_{p_ip_i}=0.4051$, $bG_{p_i\alpha_i}=0.0019$, and $b^2G_{\alpha_i\alpha_i}=0.1170$. The damping ratio of Mode 10 is also assumed to be 0.0032. The results for cases that include and ignore intermodal coupling are compared here. Without the consideration of intermodal coupling, the action of the single Mode 13 leads to a torsional flutter beyond 69.6 m/s and the action of the single Mode 10 develops a torsional flutter exceeding 74.3 m/s. The aerodynamic damping of Mode 10 is very low due to low aerodynamic damping force introduced by $A_{dii}=(2k^2)b^2A_3^*G_{\alpha_i\alpha_i}$ as compared to Mode 13. With the consideration of intermodal coupling, the curve veering of the frequency and damping loci of Modal Branches 10 and 13 is observed around 80 m/s where these two modal frequencies are close to each other. The curve veering is due to strong interactions of these two modes (Chen and Kareem 2003d). These two modal branches continuously exchange their properties as these experience veering action. As shown in Table 1, at the end of the veering action, Modal Branch 13 becomes dominated by structural Mode 10, and Modal Branch 10 is dominated by structural Mode 13. Based on Eqs. (6) and (7) and consideration of only flutter derivatives H_i^*, A_i^*, $(i=1,2,3,4)$, the coupled stiffness and damping terms involving Modes 10 and 13 are given by $A_{sij}=(2k^2)b^2A_3^*G_{\alpha_i\alpha_i}$ and $A_{dij}=(2k^2)b^2A_2^*G_{\alpha_i\alpha_j}$ with $b^2G_{\alpha_i\alpha_j}=-0.4892$. Based on the expression for the amplitude ratio, it is clear that the coupling between

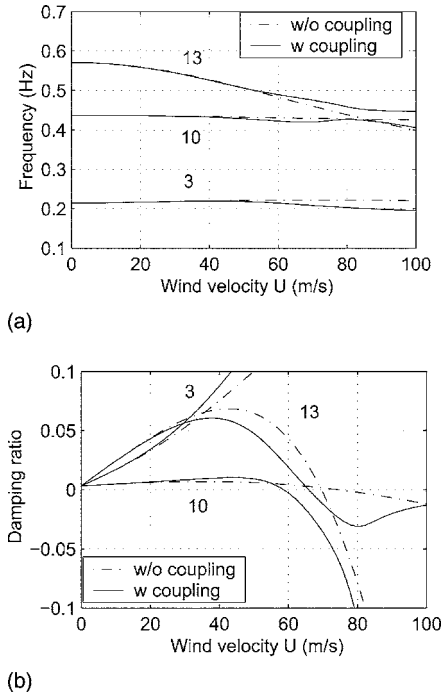

Fig. 9. Influence of intermodal coupling on torsional flutter: (a) frequency; (b) damping ratio

Modes 10 and 13 becomes significant only in the region where their frequencies are close to each other, as indicated in Table 1. This strong intermodal coupling results in a negative peak in the damping loci of Modal Branch 13 around 80 m/s. The flutter onset velocities for these two branches are 58.7 and 65.9 m/s. These results demonstrate the importance of intermodal coupling for the prediction of a torsional bridge flutter.

Influence of Drag Force on Flutter

While the self-excited drag force is often neglected in a flutter analysis, it may have a notable contribution to flutter in some cases, as observed in the case of the Akashi Kaikyo Bridge (Miyata et al. 1994). In the following, based on the proposed analysis framework, clear insight into this important issue is offered.

The following discussion focuses on the contribution of drag damping force related to $P_1^*=-2C_D/k$ (where $C_D=0.2=$static drag force coefficient). Based on Eqs. (6) and (7), the inclusion of P_1^* only affects the damping terms involving Modes 10 and 13 as

Table 1. Amplitude Ratios in Modal Branches

	Modal Branch 10		Modal Branch 13	
U (m/s)	Mode 10	Mode 13	Mode 10	Mode 13
60	1.0	0.3502	0.4182	1.0
70	1.0	0.5527	0.6548	1.0
78	1.0	0.9699	0.9921	1.0
80	1.0	1.1789	1.1378	1.0
82	1.0	1.3841	1.3225	1.0
90	1.0	1.9830	2.0711	1.0

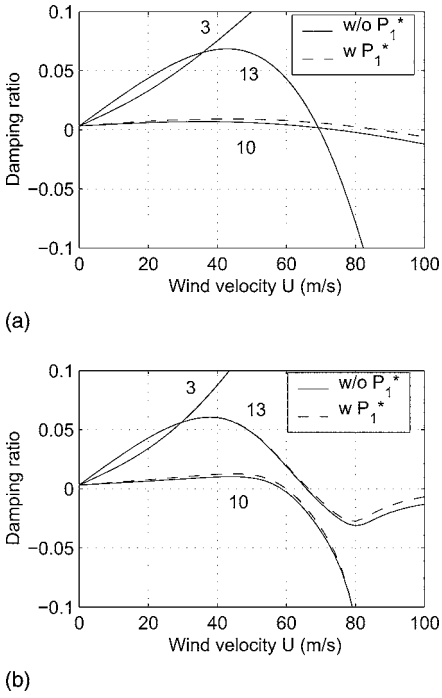

Fig. 10. Influence of drag force on flutter: (a) damping ratio (without coupling); (b) damping ratio (with coupling)

$A_{dij}=(2k^2)(P_1^*G_{p_ip_i}+b^2A_2^*G_{\alpha_i\alpha_i})$. Fig. 10(a) shows the influence of the drag force to the damping ratios in which coupling between these modes is not considered. It is noted that while the additional damping associated with the lateral motion is small, it apparently increases the onset velocity of the torsional flutter initiated from the single Mode 10 from 74.3 to 86.8 m/s. However, it has almost no influence on the torsional flutter initiated from the single Mode 13. The influence of drag force on flutter becomes negligible when the intermodal coupling of these two modes is further considered, as shown in Fig. 10(b).

This relative significance of different force components/flutter derivatives can be easily clarified based on Eqs. (6) and (7) and the framework presented in this study. The drag force may become relatively important such as in the case of soft-type flutter as demonstrated in Fig. 10(a) for Mode 10. However, the contribution of drag force will remain insignificant in the cases of hard-type flutter where aerodynamic damping generated by lift and pitching moment rapidly develops as wind velocity increases, as demonstrated in Fig. 10(a) for Mode 13 and in Fig. 10(b) for both Modal Branches 10 and 13. It is important to note that the flutter analysis framework, which offers information concerning changes in modal frequencies and damping ratios and associated mode shapes with increasing wind velocity, provides more valuable insight into the physics of multimode coupled flutter in comparison with the analysis that only focuses on the evaluation of flutter onset velocity. This information also helps to better understand the multimode coupled buffeting response of the bridge.

The importance of drag force to bridge flutter as experienced in the Akashi Kaikyo Bridge was as a result of the unique aerodynamic feature of this bridge with a truss deck section. This bridge experienced large negative angles of attack at the high wind velocity region due to its large static drag force coefficient. Around this statically displaced position, the lift and pitching moment were small and the attendant aerodynamic damping was low. In contrast, the drag force induced by torsional motion was relatively large, and its negative damping effect considerably affected the flutter performance. However, for bridges with deck sections that have low static drag force and large self-excited lift and pitching moment, the contribution of self-excited drag force is likely to be less important.

Concluding Remarks

A new analysis framework that offers closed-form expressions for estimating modal characteristics of bimodal coupled bridge systems and for estimating onset of flutter was presented. The flutter analysis of a cable-stayed bridge demonstrated the accuracy and effectiveness of the proposed framework comparable to the conventional framework using numerical complex eigenvalue analysis. The only assumption made in the proposed framework was low level of damping, which has also been implicitly invoked in the modeling of the self-excited forces and analysis of bridge flutter using conventional numerical approaches. Hence, this assumption is by no means restrictive, thus the proposed framework is applicable to a variety of bimodal coupled systems. At the flutter onset velocity with zero damping, the proposed framework gives the exact solution of flutter as the conventional eigenvalue analysis because the invoked approximation vanishes.

The proposed framework offered intuitive and valuable insight into the significance of structural and aerodynamic characteristics of coupled bridge flutter without performing extensive numerical parametric studies as needed in the traditional framework. It clearly pointed to the dominant role of coupled self-excited forces in the generation of negative damping that led to bridge flutter instability. These insights aided in better understanding the underlying physics of bridge flutter and offered better measures for tailoring of bridge deck sections and effective selection of structural systems for superior flutter performance.

The proposed framework also helped to guide in the selection of critical structural modes in a multimode flutter analysis. A mode comprised of large values of coupled aerodynamic stiffness and damping terms with the fundamental torsional mode is more likely to be important to bridge flutter. This intermodal coupling will be enhanced when its damping is low and its frequency is close to the torsional modal frequency. Some modes may become locally important to flutter at a certain wind velocity region when their frequencies fall close to the torsional mode frequency. The understanding of modes that play a major role in flutter equally offers valuable information for the design and interpretation of wind tunnel studies using full aeroelastic bridge models where only limited modes of vibration can be physically modeled.

The flutter analysis of a cable-stayed bridge with a relatively bluff section pointed out the potential importance of intermodal aerodynamic coupling in the prediction of torsional flutter. The intermodal coupling may meaningfully affect the flutter onset velocity, particularly, in soft-type flutter cases where the aerodynamic damping generated by the lift and pitching moment slowly builds up with increasing wind velocity. This necessitates the use of a multimode coupled analysis framework for the prediction of even torsional flutter, which has been customarily analyzed by using the traditional mode-by-mode approach.

Clear insight into the significance of different force components/flutter derivatives such as drag force to flutter was provided. The drag force may become relatively important for soft-type flutter cases. However, its contribution will remain insignificant for hard-type flutter cases where aerodynamic damping caused by the self-excited lift and pitching moment rapidly devel-

ops as the wind velocity increases. It was emphasized that the flutter analysis framework that offered information concerning delineation of changes in modal frequencies and damping ratios and associated mode shapes with increasing wind velocity provided more valuable insights into the underlying physics of multimode coupled flutter as compared to the analysis that only focused on the determination of flutter onset velocity. This information also helps to better understand the multimode coupled buffeting response of the bridge.

Acknowledgments

The support for this work was provided in part by NSF Grant No. CMS 03-24331. This support is gratefully acknowledged. The first writer also gratefully acknowledges the support of the new faculty start-up funds provided by Texas Tech University.

References

Chen, X., and Kareem, A. (2002). "Advances in modeling of aerodynamic forces on bridge decks." *J. Eng. Mech.*, 128(11), 1193–1205.

Chen, X., and Kareem, A. (2003a). "Aeroelastic analysis of bridges: Effects of turbulence and aerodynamic nonlinearities." *J. Eng. Mech.*, 129(8), 885–895.

Chen, X., and Kareem, A. (2003b). "New frontiers in aerodynamic tailoring of long span bridges: An advanced analysis framework." *J. Wind. Eng. Ind. Aerodyn.*, 91(12-15), 1511–1528.

Chen, X., and Kareem, A. (2003c). "Efficacy of tuned mass dampers for bridge flutter control." *J. Struct. Eng.*, 129(10), 1291–1300.

Chen, X., and Kareem, A. (2003d). "Curve veering of eigenvalue loci of bridges with aeroelastic effects." *J. Eng. Mech.*, 129(2), 146–159.

Chen, X., Matsumoto, M., and Kareem, A. (2000a). "Aerodynamic coupling effects on flutter and buffeting of bridges." *J. Eng. Mech.*, 126(1), 17–26.

Chen, X., Matsumoto, M., and Kareem, A. (2000b). "Time domain flutter and buffeting response analysis of bridges." *J. Eng. Mech.*, 126(1), 7–16.

Diana, G., Cheli, F., Zasso, A., and Bocciolone, M. (1999). "Suspension bridge response to turbulent wind: Comparison of new numerical simulation method results with full scale data." *Wind Engineering into the 21st century*, A. Larsen, G. L. Larose, and F. M. Livesey, eds., Balkema, Rotterdam, The Netherlands, 871–878.

Jones, N. P., Raggett, J. D., and Ozkan, E. (2002). "Prediction of cable-supported bridge response to wind: Coupled flutter assessment during retrofit." *J. Wind. Eng. Ind. Aerodyn.*, 91(12-15), 1445–1464.

Jones, N. P., Scanlan, R. H., Jain, A., and Katsuchi, H. (1998). "Advances (and challenges) in the prediction of long-span bridge response to wind." *Bridge aerodynamics*, A. Larsen and S. Esdahl, eds., Balkema, Rotterdam, The Netherlands, 59–85.

Matsumoto, M. (1999). "Recent study on bluff body aerodynamics and its mechanism." *Wind engineering into the 21st century*, A. Larsen, G. L. Larose, and F. M. Livesey, eds., Balkema, Rotterdam, The Netherlands, 67–78.

Matsumoto, M., Daito, Y., Yoshizumi, F., Ichikawa, Y., and Yabutani, T. (1997). "Torsional flutter of bluff bodies." *J. Wind. Eng. Ind. Aerodyn.*, 69-71(0), 871–882.

Miyata, T., Tada, K., Sato, H., Katsuchi, H., and Hikami, Y. (1994). "New findings of coupled flutter in full model wind tunnel tests on the Akashi Kaikyo Bridge." *Proc., Symp. on Cable-Stayed and Suspension Bridges*, Deauville, France, October 12–15, 163–170.

Scanlan, R. H. (1978). "The action of flexible bridges under wind. 1: Flutter theory." *J. Sound Vib.*, 60(2), 187–199.

Scanlan, R. H. (1993). "Problematics in formulation of wind-force models for bridge decks." *J. Eng. Mech.*, 119(7), 1353–1375.